STEM CELLS TRANSLATIONAL MEDICINE®

TISSUE ENGINEERING AND REGENERATIVE MEDICINE

Enhanced Osteogenesis of Adipose-Derived Stem Cells by Regulating Bone Morphogenetic Protein Signaling Antagonists and Agonists

JIABING FAN,[a] CHOONG SUNG IM,[a] MIAN GUO,[b] ZHONG-KAI CUI,[a] ARMITA FARTASH,[c] SOYON KIM,[d] NIKHIL PATEL,[a] OLGA BEZOUGLAIA,[c] BENJAMIN M. WU,[a,d] CUN-YU WANG,[e] TARA L. AGHALOO,[c,*] MIN LEE[a,d,*]

Key Words. Adipose-derived stem cells • Noggin • Phenamil • BMP–Smad signaling • Osteogenesis

[a]Division of Advanced Prosthodontics, School of Dentistry, [c]Division of Diagnostic and Surgical Sciences, School of Dentistry, [d]Department of Bioengineering, and [e]Division of Oral Biology and Medicine, School of Dentistry, University of California, Los Angeles, Los Angeles, California, USA; [b]Department of Neurosurgery, 2nd Affiliated Hospital of Harbin Medical University, Harbin, Heilonjiang, People's Republic of China

[*]Contributed equally.

Correspondence: Min Lee, Ph.D., Division of Advanced Prosthodontics, UCLA School of Dentistry, 10833 Le Conte Avenue, CHS 23-088F, Los Angeles, California 90095-1668, USA. Telephone: 310-825-6674; E-Mail: leemin@ucla.edu; or Tara L. Aghaloo, D.D.S., M.D., Ph.D., Division of Diagnostic and Surgical Sciences, UCLA School of Dentistry, 10833 Le Conte Avenue, CHS 53-009, Los Angeles, California 90095-1668, USA. Telephone: 310-206-6766; E-Mail: taghaloo@dentistry.ucla.edu

Received September 14, 2015; accepted for publication November 9, 2015; published Online First on March 8, 2016.

1066-5099/2016/$20.00/0

http://dx.doi.org/10.5966/sctm.2015-0249

ABSTRACT

Although adipose-derived stem cells (ASCs) are an attractive cell source for bone tissue engineering, direct use of ASCs alone has had limited success in the treatment of large bone defects. Although bone morphogenetic proteins (BMPs) are believed to be the most potent osteoinductive factors to promote osteogenic differentiation of ASCs, their clinical applications require supraphysiological dosage, leading to high medical burden and adverse side effects. In the present study, we demonstrated an alternative approach that can effectively complement the BMP activity to maximize the osteogenesis of ASCs without exogenous application of BMPs by regulating levels of antagonists and agonists to BMP signaling. Treatment of ASCs with the amiloride derivative phenamil, a positive regulator of BMP signaling, combined with gene manipulation to suppress the BMP antagonist noggin, significantly enhanced osteogenic differentiation of ASCs through increased BMP–Smad signaling in vitro. Furthermore, the combination approach of noggin suppression and phenamil stimulation enhanced the BMP signaling and bone repair in a mouse calvarial defect model by adding noggin knockdown ASCs to apatite-coated poly(lactic-coglycolic acid) scaffolds loaded with phenamil. These results suggest novel complementary osteoinductive strategies that could maximize activity of the BMP pathway in ASC bone repair while reducing potential adverse effects of current BMP-based therapeutics. STEM CELLS TRANSLATIONAL MEDICINE *2016;5:539–551*

SIGNIFICANCE

Although stem cell-based tissue engineering strategy offers a promising alternative to repair damaged bone, direct use of stem cells alone is not adequate for challenging healing environments such as in large bone defects. This study demonstrates a novel strategy to maximize bone formation pathways in osteogenic differentiation of mesenchymal stem cells and functional bone formation by combining gene manipulation with a small molecule activator toward osteogenesis. The findings indicate promising stem cell-based therapy for treating bone defects that can effectively complement or replace current osteoinductive therapeutics.

INTRODUCTION

Bone defects caused by traumatic injury, tumor extirpation, and degenerative diseases are challenging health problems [1]. A cell-based tissue-engineering strategy offers a promising alternative to repair or regenerate the damaged bone [2]. Although mesenchymal stem cells (MSCs) derived from adipose tissues are a readily available cell source for bone tissue engineering, direct use of adipose-derived stem cells (ASCs) alone has had limited success in the repair of large bone defects [3, 4]. Thus, there is an increasing interest in employing the use of osteoinductive factors to enhance osteogenesis of ASCs [5, 6]. Although bone morphogenetic proteins (BMPs) are considered the most potent osteoinductive factors, supraphysiological dosage of BMPs is required for clinical bone treatment, which would increase the medical cost and could cause undesired adverse effects such as life-threatening tissue swelling, ectopic bone, and cancer [7–12]. To provide a safe and cost-efficient treatment, it is necessary to establish an alternative osteoinductive strategy that can effectively complement the activity of BMP in osteogenesis of ASCs.

One potential approach is to deliver no exogenous BMPs, while enhancing endogenous BMP activities in ASC osteogenesis by inhibiting negative regulators of BMP signaling. BMP

signaling is negatively regulated by various extramembranous and intracellular antagonists such as noggin, chordin, gremlin, and ubiquitin ligase Smad ubiquitination regulatory factor (Smurf1) [13, 14]. Noggin is a BMP antagonist by interfering with BMP binding to its cell receptors [15–17]. In response to BMPs, osteoblastic cells were revealed to upregulate the expression of noggin as part of a negative feedback loop to regulate increased levels of BMP signaling [18]. Several studies previously reported that the application of exogenous noggin impaired both in vitro osteogenesis and in vivo bone formation, whereas use of noggin-neutralizing antibodies improved bone repair [19–21]. We recently reported that noggin knockdown enhanced BMP-induced osteogenesis of ASCs in vitro and bone formation in vivo [22, 23].

The potency of endogenous BMP signaling can be further enhanced by delivering small molecule compounds that can induce osteogenic differentiation through BMP–Smad signaling, such as phenamil. In comparison with growth factor proteins, small osteoinductive molecules present several advantages such as relatively low cost (easy synthesis), high stability, and low immunogenicity [24]. The small molecule phenamil, a derivative of the U.S. Food and Drug Administration-approved diuretic amiloride, is currently attracting attention in bone regeneration due to its osteogenic efficacy through the BMP–Smad signaling pathways [25]. Phenamil induces osteogenic differentiation in mouse bone marrow stromal or preosteoblastic cells and human dental pulp cells [26, 27]. We recently reported the osteogenic activity of phenamil in vitro and bone formation in vivo in a calvarial defect model, both alone and in combination with BMP-2 utilizing a reduced BMP-2 dose [28]. The osteogenic activity of phenamil has been reported to be mediated by downregulating BMP antagonist Smurf1 and stabilizing Smads through induction of tribbles homolog 3 (Trb3), thereby stimulating BMP signaling [25, 28, 29].

Here, we seek to enhance BMP–Smad signaling by inhibiting expression of a BMP antagonist (noggin) and delivering a small molecule activator of BMP signaling (phenamil) for maximal ASC osteogenesis without exogenous application of BMPs. We downregulated noggin in ASCs using an RNA interference strategy, and their osteogenic differentiation through BMP–Smad signaling was evaluated with phenamil treatment in vitro. We further investigated the complementary approach of noggin suppression and phenamil stimulation to enhance the BMP–Smad signaling and bone repair in a calvarial defect model using apatite-coated poly(lactic-coglycolic acid) (Ap-PLGA) scaffold loaded with noggin knockout ASCs and phenamil. Our study demonstrated that the combination of noggin suppression and phenamil treatment is an effective strategy to enhance osteogenesis of ASCs; such a strategy could maximize activity of BMP–Smad pathway in bone regeneration while minimizing BMP-mediated adverse effects.

Materials and Methods

Animals

All animal studies were performed by using protocols approved by the University of California, Los Angeles (UCLA) Animal Research Committee and were in compliance with Guidelines for the Care and Use of Laboratory Animals of the National Institutes of Health.

Isolation and Culture of ASCs

Cells were harvested from inguinal fat pads of male C57BL/6 mice (Charles River Laboratories, Wilmington, MA, http://www.criver.com) at the age of 4–8 weeks, according to previous protocols established, because these cells were shown to differentiate into osteogenic lineage in our previous studies [22, 23]. The collected adipose tissues were rinsed in sterile phosphate-buffered saline (PBS), cut into small pieces, and then digested with 0.1% collagenase type I (Sigma-Aldrich, St. Louis, MO, http://www.sigmaaldrich.com). After 2 hours of digestion, cells were released from adipose tissues and were subjected to centrifugation at 1,200 rpm for 5 minutes. Finally, the cells were resuspended in growth medium including low-glucose Dulbecco's Modified Eagle's Medium (Life Technologies, Grand Island, NY, http://www.thermofisher.com), 10% fetal bovine serum (FBS; Life Technologies), and 1% penicillin/streptomycin (Life Technologies). The ASCs at passage 3 were used for further studies.

Gene Transduction

Lentiviral particles (Santa Cruz Biotechnology, Dallas, TX, http://www.scbt.com) containing short hairpin RNA (shRNA) targeting noggin gene were used to transduce ASCs according to the manufacturer's instructions. Briefly, the cells were seeded onto six-well plates and cultured until 50% confluence. The mixture of shRNA lentiviral particles and polybrene (8 μg/ml; Sigma-Aldrich) was then added to the culture medium and incubated overnight. Stable clones expressing shRNA were selected with puromycin dihydrochloride (Sigma-Aldrich). Cells transduced with lentiviral particles containing a scrambled shRNA sequence served as negative controls.

Alkaline Phosphatase Activity and Alizarin Red Staining

Cells were cultured in 12-well plates with growth medium. After 100% confluence, the medium was replaced with an osteogenic medium containing 10 mM β-glycerophosphate (Sigma-Aldrich), 50 μg/ml L-ascorbic acid (Sigma-Aldrich), 100 nM dexamethasone (Sigma-Aldrich), and phenamil (Sigma-Aldrich) at various concentrations (0, 5, 10, or 20 μM). After 3 days of culture, alkaline phosphatase (ALP) was stained as previously described [22]. In brief, cells were fixed in 10% formalin, rinsed with PBS, and incubated in a solution containing Nitro Blue tetrazolium (Sigma-Aldrich) and 5-bromo-4-chloro-3-indoxylphosphate (Sigma-Aldrich) stock solutions in AP buffer (100 mM Tris, pH 8.5, 50 mM $MgCl_2$, 100 mM NaCl) for 1 hour. The stained samples were visualized with the Olympus BX 51 microscope (Olympus, Center Valley, PA, http://www.olympusamerica.com). ALP staining was further quantified by ImageJ software (NIH, Bethesda, MD). For the colorimetric measurement of ALP activity, cells were lysed in 0.2% NP-40 lysis buffer (Life Technologies) and measured at the absorbance of 405 nm by using *p*-nitrophenol phosphate substrate (Sigma-Aldrich). Measurements were normalized to total DNA content evaluated by the PicoGreen dsDNA Assay (Life Technologies).

Calcium deposition was evaluated by using alizarin red staining as previously described [22]. After 14 days, the fixed cells were incubated in 2% alizarin red staining solution (Sigma-Aldrich) for 5 minutes. The stained samples were observed with an Olympus BX 51 microscope. To quantify mineralization, the stained cells

were dissolved in 10% (vol/vol) acetic acid and measured at the absorbance of 405 nm.

RNA Extraction and Quantitative Real-Time Polymerase Chain Reaction

Cellular RNA extraction was performed with TRIzol reagent (Life Technologies) and RNeasy Mini Plant kit (Qiagen, Valencia, CA, https://www.qiagen.com) as previously described [22]. Briefly, 0.5 μg of total RNA was reverse-transcribed to cDNA by using a cDNA transcription kit (Life Technologies). Quantitative real-time polymerase chain reaction (qRT-PCR) was analyzed by using LightCycler 480 PCR (Roche, Indianapolis, IN, http://www.roche.com) with 20 μl of SYBR Green reaction system. PCR amplification was run for 45 cycles. *GAPDH* expression level was used to normalize other gene expression levels. The following primers were used in this experiment: *Runx2*: CGGTCTCCTTCAGGATGGT (forward), GCTTCCGTCAGCGTCAACA (reverse); *Osterix*: GCTAGAGATCTGAGCCGGGTA (forward), AAGAGAGCCTGGCAAGAGG (reverse); *ALP*: GTTGCCAAGCTGGGAAGAACAC (forward), CCCACCCCGCTATTCCAAAC (reverse); *Osteopontin* (*OPN*): CTCCTGG CTGAATTCTGAGG (forward), TGCCAGAATCAGTCA CTTTCA (reverse); *Collagen1a1* (*Col1a*): AACCCGAGGTATGCTTGATCT (forward), CC AGTTCTTCATTGCATTGC (reverse); *Osteocalcin* (*OCN*): GGGAGACAACAGGGAGGAAAC (forward), CAGGCTTCCTGCCAGTACCT (reverse); *Noggin*: CCGGGCTTTATGGCTACTTC (forward), TCCAGCCCTTTGATCTCG (reverse); *Trb3*: CTGAGGCTCCAGGACAAGA (forward), CCTGCAGGAAACATCAGCA (reverse); *GAPDH*: AGGTCGGTGTGAACGGATTTG (forward), TGTAGACCATGTAGTTGAGGTCA (reverse).

Western Blot Analysis

The Western blot assay was performed as previously described [28]. In brief, after cells were lysed in 0.2% NP-40 lysis buffer, total cellular protein concentration was measured by using bicinchoninic acid protein assay (Thermo Scientific, Rockford, IL, http://www.thermoscientific.com). The proteins were separated with SDS-polyacrylamide gel electrophoresis, blotted onto Immobilon polyvinyl difluoride membrane (Millipore, Billerica, MA, http://www.emdmillipore.com), and detected with polyclonal antibodies (Santa Cruz Biotechnology) for Noggin, Trb3, Smurf1, Smad5, pSmad1/5/8, and GAPDH. The membranes were then incubated with horseradish peroxidase (HRP)-conjugated secondary antibody (Millipore). The immunoreactive proteins were subsequently visualized with chemiluminescent HRP (Denville Scientific, South Plainfield, NJ, http://www.denvillescientific.com).

Luciferase Assay

Id1 luciferase reporter assay was performed as previously described [30]. Briefly, cells at 70%–80% confluence were cotransfected with pGL4[luc2P/hID1/Hygro] Vector (Promega, Fitchburg, WI, http://www.promega.com) and Renilla control vector (Promega) by using Lipofectamine 2000 (Life Technologies). After transfection for 6 hours, cells were treated with 20 μM phenamil. After 48 hours of treatment, luciferase activities were measured by using a dual luciferase reporter system (Promega) and normalized with Renilla internal control values.

Preparation of Scaffolds

PLGA scaffolds were fabricated by the solvent casting and particulate leaching technique as previously described [31, 32]. Sucrose of 200- to 300-μm diameter was mixed with PLGA/chloroform solution to reach 92% porosity (volume fraction) and compressed into thin sheets with Teflon plates. Scaffolds were freeze-dried to eliminate the residual solvents at 100 mTorr and -110°C (SP Industries, Warminster, PA, http://www.spindustries.com) overnight. Sucrose was subsequently leached by immersing scaffolds in double-distilled (dd) H_2O. Then scaffolds were sterilized by immersion in 70% ethanol for 30 minutes, followed by three rinses of sterile ddH_2O. Finally, the scaffold sheets were punched into 3-mm-diameter discs for further applications.

Biomimetic Apatite Coating Process

Apatite coating solution was prepared as described in previous studies [31, 32]. Briefly, simulated body fluids (SBF) were formulated by sequentially dissolving $CaCl_2$, $MgCl_2{\cdot}6H_2O$, $NaHCO_3$, and $K_2HPO_4{\cdot}3H_2O$ into ddH_2O. Adjustment of pH was made to 6.0, and then Na_2SO_4, KCl, and NaCl were dissolved. The final solution was brought to a pH of 6.5 (SBF1). Mg^{2+} and HCO_3^- free SBF (SBF2) was prepared by similarly dissolving $CaCl_2$ and $K_2HPO_4{\cdot}3H_2O$ into ddH_2O and pH was adjusted to 6.0. KCl and NaCl were added, and the solution was adjusted to pH 6.8. All solutions were sterile filtered by using a 0.22-μm polyethersulfone membrane (Nalgene, Rochester, NY, http://nalgene.com). The scaffold discs were subjected to glow discharge argon plasma etching (Harrick Scientific, Pleasantville, NY, http://www.harrickssci.com). The etched scaffolds were immersed and incubated in SBF1 for 24 hours and then further incubated in SBF2 for another 24 hours at 37°C. The apatite-coated scaffolds were washed with sterile ddH_2O to remove excess ions and lyophilized before further studies.

Scanning Electron Microscopy

The internal morphology of Ap-PLGA scaffold was investigated by scanning electron microscopy (Nova NanoSEM 230; FEI, Hillsboro, OR, http://www.fei.com). The cross-sectioned samples were mounted on aluminum stubs and sputter-coated with gold at 20 mA under 70 mTorr for 50 seconds.

Release of Phenamil From Scaffolds

The release profile of Phenamil was analyzed as described previously [28]. Briefly, phenamil was adsorbed onto scaffolds at a final concentration of 300 μM and lyophilized in a freeze dryer for 3 hours. The phenamil-loaded scaffolds were incubated in 1 ml of PBS (pH 7.4) supplemented with 10% FBS at 37°C. The whole incubating solution was removed and replenished with 1 ml of fresh solution at predetermined time points over a span of 21 days. The amount of released phenamil was evaluated by UV spectrometry at an absorbance of 366 nm.

The bioactivity of phenamil released from the scaffolds was assessed by measuring its ability to increase ALP activity in ASCs. Phenamil-loaded scaffolds were incubated in the osteogenic medium for 3 days, and the supernatant was collected for the assay. Freshly reconstituted phenamil was used as a control. ASCs were seeded onto 96-well plates at the final concentration of 1,000 cells per well and cultured in growth medium. At the beginning of the assay, the medium was replaced with osteogenic

medium supplemented with the scaffold supernatant at final phenamil concentration of 20 μM. After incubation for 3 days, ALP activity was determined colorimetrically according to the methods described above.

Cell Proliferation and Differentiation on Scaffolds

To visualize the cell proliferation on the scaffolds, cell were seeded onto apatite-coated PLGA scaffolds at the final concentration of 2×10^6 cells per milliliter, stained with a Live/Dead staining kit (Life Technologies) at 37°C for 15 minutes, and observed under a fluorescence microscope (Olympus) at days 1 and 14. To quantify the cell proliferation on the scaffolds, the cell/scaffold constructs were analyzed with the AlamarBlue assay kit (Life Technologies) at days 1, 3, 7, and 14. Briefly, the cell/scaffold constructs were rinsed with PBS and incubated with sterilized 10% AlamarBlue solution for 3 hours at 37°C. AlamarBlue fluorescence was measured at 535 nm (excitation) and 600 nm (emission). To measure the osteogenic differentiation, cells on the scaffolds were cultured with the osteogenic medium and measured colorimetrically by ALP activity at day 3 according to the methods described above.

Calvarial Defect Model

The calvarial defect model was performed in 2-month-old male CD-1 nude mice (Charles River) to minimize the host immune responses to implanted cells. Calvaria of mice were trephine drilled with constant irrigation to create 3-mm full-thickness craniotomy defects in each parietal bone without damaging the underlying dura mater as previously described [28]. Ap-PLGA scaffolds loaded with or without phenamil (300 μM) were seeded with either control shRNA or noggin shRNA-transduced ASCs. After implantation, all animals were placed on a warm sheet for recovery and then transferred to the vivarium for postoperative care. For postoperative treatment, all mice received subcutaneous injections of buprenorphine at the concentration of 0.1 mg/kg for 3 days.

Three-Dimensional Microcomputed Tomography Scanning

At 6 weeks after implantation, animals were sacrificed, and calvarial tissues were harvested for further analysis. The extracted calvarial tissues were fixed in 4% formaldehyde at room temperature with gentle shaking. After 48 hours of fixation, the samples were rinsed with PBS and stored in 70% ethanol at 4°C before imaging using the high-resolution microcomputed tomography (microCT) machine (microCT SkyScan 1172; Bruker MicroCT, Kontich, Belgium, http://bruker-microct.com) using 57 kVp, 184 μA, 0.5-mm aluminum filtration, and 10-μm resolution. All data were visualized and reconstructed by using Dolphin 3D software (Dolphin Imaging & Management Solutions, Chatsworth, CA, http://www.dolphinimaging.com). New bone volume and area were analyzed by using CTAn (Bruker MicroCT) and ImageJ software. Bone specific analysis included new bone area/original defect size (percent area), new bone volume/tissue volume (percent BV/TV), and trabecular number ($TN \cdot mm^{-1}$).

Histological and Immunohistochemical Analyses

The fixed calvarial bone tissues were decalcified in 10% EDTA solution with gentle shaking for 1 week. Decalcified samples were embedded in paraffin and cut into sections of 5-μm thickness. The tissue sections were deparaffinized and stained with hematoxylin and eosin (H&E). The deparaffinized slides were further stained with 0.1% PicroSirius red solution (Polysciences, Inc., Warrington, PA, http://www.polysciences.com) and observed under polarizing light microscope. Masson's trichrome staining was also used to detect new bone formation stained with light green color. Additional sections were analyzed by immunohistochemistry. The deparaffinized sections were treated by using citric acid antigen retrieval, incubated with the primary antibodies (Santa Cruz Biotechnology) including Noggin, Trb3, pSmad1/5/8, Runx2, and OCN, and stained by HRP/3,3′-diaminobenzidine detection kit (Abcam, Cambridge, MA, http://www.abcam.com) according to the manufacturer's instructions. The sections were further counterstained with Mayer's hematoxylin (Abcam). The three random areas in each image were further quantified by ImageJ software.

Statistical Analysis

Statistical analysis was performed by using one-way analysis of variance, with the Tukey's post hoc test when more than two groups were compared. Student's *t* test was used to compare two groups. The data were presented as means $\pm$ SD. $p < .05$ was considered statistically significant.

RESULTS

Osteogenic Differentiation of ASCs by Noggin Suppression and Phenamil

The effects of noggin suppression and phenamil on osteogenesis was investigated in ASCs transduced with noggin shRNA or control shRNA at various concentrations of phenamil (0, 5, 10, or 20 μM) (Fig. 1). Early osteogenic differentiation was detected by ALP staining and quantification after 3 days of ASC culture (Fig. 1A, 1B). Phenamil treatment dose-dependently increased the expression of ALP as the phenamil concentration increased from 5 to 20 μM, and noggin suppression further increased the ALP expression in ASCs. The ALP expression was significantly higher in ASCs treated with noggin shRNA and 20 μM phenamil compared with the one detected in ASCs with control shRNA (Fig. 1B).

The expression of osteogenic differentiation markers including *Runx2*, *Osterix*, *Col1a*, *ALP*, *OPN*, and *OCN* was examined with qRT-PCR (Fig. 1C). Noggin shRNA increased the expression of *Osterix* and *Runx*2, major transcription genes to regulate osteogenic differentiation, 5.8- and 1.7- fold, respectively. When further stimulated with 20 μM phenamil, the *Osterix* and *Runx*2 expression level increased 33.8- and 3.8-fold, respectively, compared with ASCs without phenamil treatment. ASCs treated with noggin shRNA and 20 μM phenamil showed significant increase on the *ALP* expression, confirming the results of ALP staining. The expression levels of *Col1a*, *OPN*, and *OCN* were significantly increased by noggin suppression, with strong promotion of these genes when supplemented with phenamil (Fig. 1C).

Finally, the end-stage osteogenesis was investigated by observing extracellular matrix mineralization through alizarin red staining on day 14 (Fig. 1D). The noggin suppression increased the extent of mineralization in ASCs by 1.4-fold in the absence of phenamil (Fig. 1E). Phenamil treatment (from 5 to 20 μM) dose-dependently increased mineralization of ASCs treated with

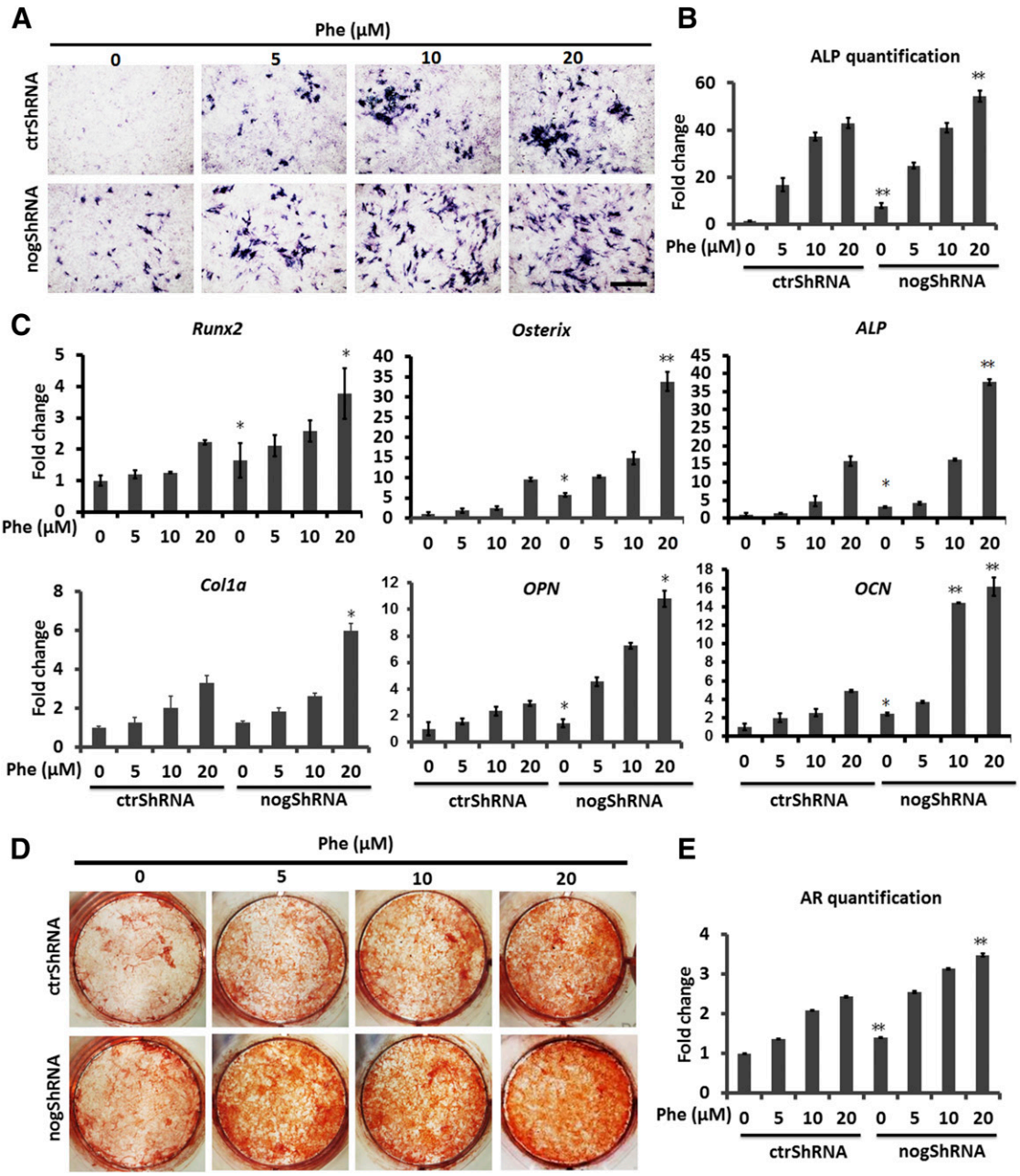

Figure 1. Noggin suppression and phenamil enhance osteogenic differentiation of ASCs in monolayer culture. Osteogenic markers were assessed in ASCs transduced with noggin shRNA or control shRNA in the presence or absence of phenamil. **(A, B):** ALP expression was measured by ALP staining and quantification at day 3. Scale bar = 500 μm. **(C):** Osteogenic gene expression including *Runx2*, *Osterix*, *ALP*, *Col1a*, *OPN*, and *OCN*, as analyzed by quantitative real-time polymerase chain reaction at day 3. Upregulation of all genes was noted in noggin shRNA cells in the presence of phenamil. **(D, E):** Extracellular matrix mineralization was increased in noggin shRNA cells in the presence or absence of phenamil as measured by AR staining and quantification at day 14. Data are presented as means ± SD ($n = 3$ per group). ∗, $p < .05$, ∗∗, $p < .01$ versus control shRNA. Abbreviations: AR, alizarin red; ASCs, adipose-derived stem cells; ALP, alkaline phosphatase; Col1a, Collagen1a1; ctrShRNA, control shRNA; nogShRNA, Noggin shRNA; OCN, osteocalcin; OPN, osteopontin; Phe, phenamil; shRNA, short hairpin RNA.

control shRNA by 1.4- to 2.4-fold, which was further increased with noggin suppression by 2.6- to 3.5-fold (Fig. 1E).

BMP Signaling in ASCs Enhanced by Noggin Suppression and Phenamil

To understand the molecular mechanisms involved in osteogenesis induced by noggin suppression and phenamil, we investigated the expression of noggin in ASCs with or without phenamil stimulation. qRT-PCR results showed that ASCs with noggin shRNA transduction decreased the transcriptional level of the *noggin* gene by threefold in the presence and absence of phenamil, compared with ASCs transduced with control shRNA (Fig. 2A). We then investigated the expression level of *Trb3* because phenamil has been demonstrated to enhance BMP signaling through upregulation of *Trb3* (Fig. 2B). Phenamil treatment increased the mRNA level of *Trb3*

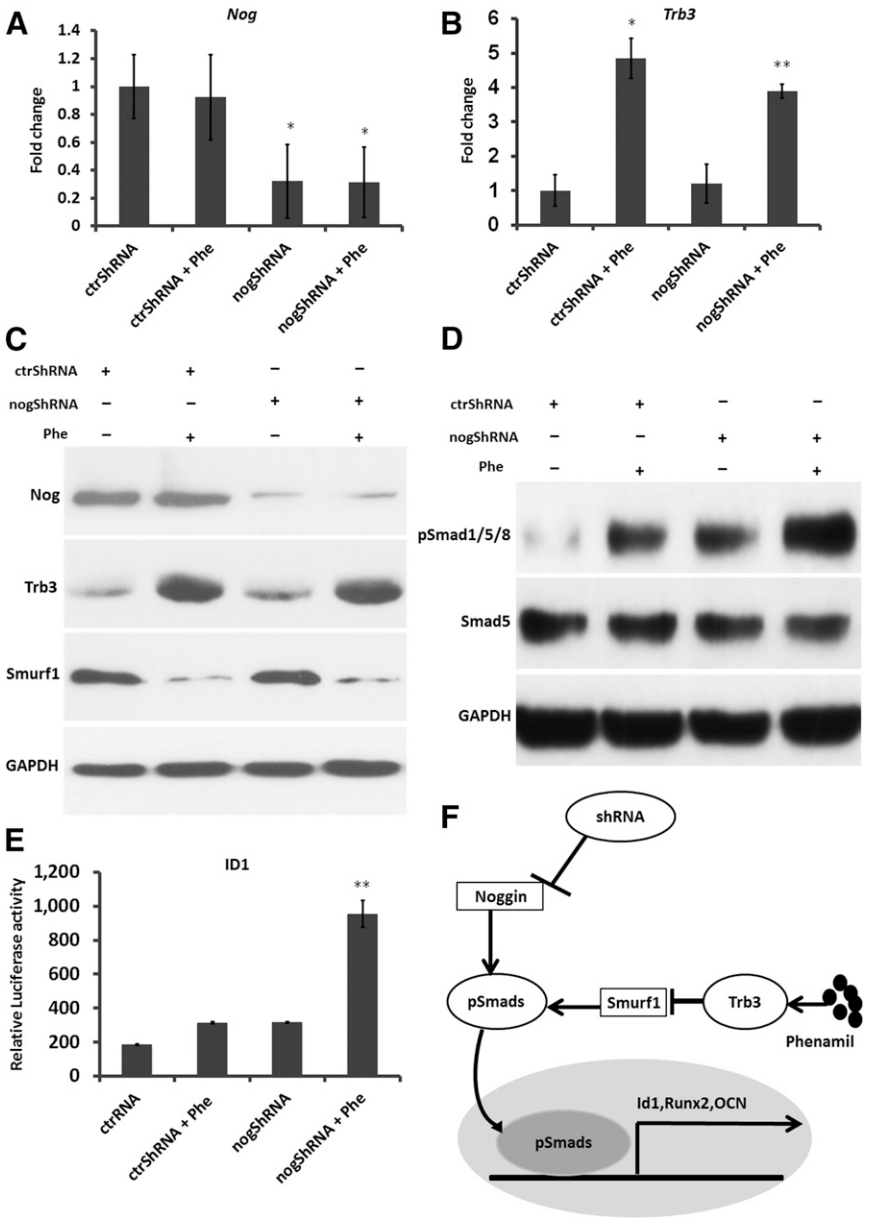

Figure 2. Noggin suppression and phenamil stimulates BMP–Smad signaling pathway. **(A):** *Noggin* expression was downregulated in noggin shRNA-treated ASCs as measured by real-time PCR. **(B):** Phenamil-induced expression of *Trb3* in ASCs as measured by real-time PCR. **(C):** Western blot analysis of Noggin, Trb3, Smurf1 at 24 hours. **(D):** Western blot analysis of Smad5, pSmad1/5/8 at 24 hours. **(E):** Id1 promoter activity was measured by luciferase assay. **(F):** Schematic diagram of the mechanism for the enhanced BMP–Smad signaling pathway by noggin suppression and phenamil. Noggin suppression enhanced BMP–Smad signaling by increasing the phosphorylation of Smad 1/5/8 that was subsequently stimulated by phenamil-induced Trb3 to reduce Smurf1 expression. Data presented as means ± SD (n = 3 per group). ∗, $p < .05$, ∗∗, $p < .01$ versus control shRNA. Abbreviations: ASCs, adipose-derived stem cells; BMP, bone morphogenetic protein; ctrShRNA, control shRNA; nogShRNA, Noggin shRNA; *Nog*, *Noggin*; OCN, osteocalcin; PCR, polymerase chain reaction; Phe, phenamil; shRNA, short hairpin RNA; Smurf1, ubiquitin ligase Smad ubiquitination regulatory factor; Trb3, tribbles homolog 3.

by 3.9- to 4.9-fold with or without noggin suppression. There was no significant effect of noggin suppression on *Trb3* expression (Fig. 2B). Next, the effects of noggin suppression and phenamil on BMP-Smad signaling were evaluated by Western blot for Noggin, Trb3, Smurf1, and phosphorylated Smads (pSmad1/5/8) (Fig. 2C, 2D). The downregulation of noggin protein expression was confirmed in ASCs treated with noggin shRNA in the presence or absence of phenamil. Furthermore, Trb3 protein expression was significantly increased with phenamil treatment, regardless of the presence of noggin shRNA. The increased amount of Trb3 downregulated the expression of Smurf1, which in turn enhanced the expression level of pSmad1/5/8, which are major signal transducers for BMP (Fig. 2C, 2D). Most importantly, ASCs treated with noggin shRNA and phenamil led to promote strong expression in pSmad1/5/8 (Fig. 2D). We further confirmed the combined effects of noggin suppression and phenamil treatment on BMP–Smad signaling by examining the promoter activity of BMP-target gene Id1 using luciferase reporter assay (Fig. 2E). Id1 is one of the major downstream targets of BMP signaling, and the BMP-induced Id1 expression was shown to be mediated by binding Smad proteins

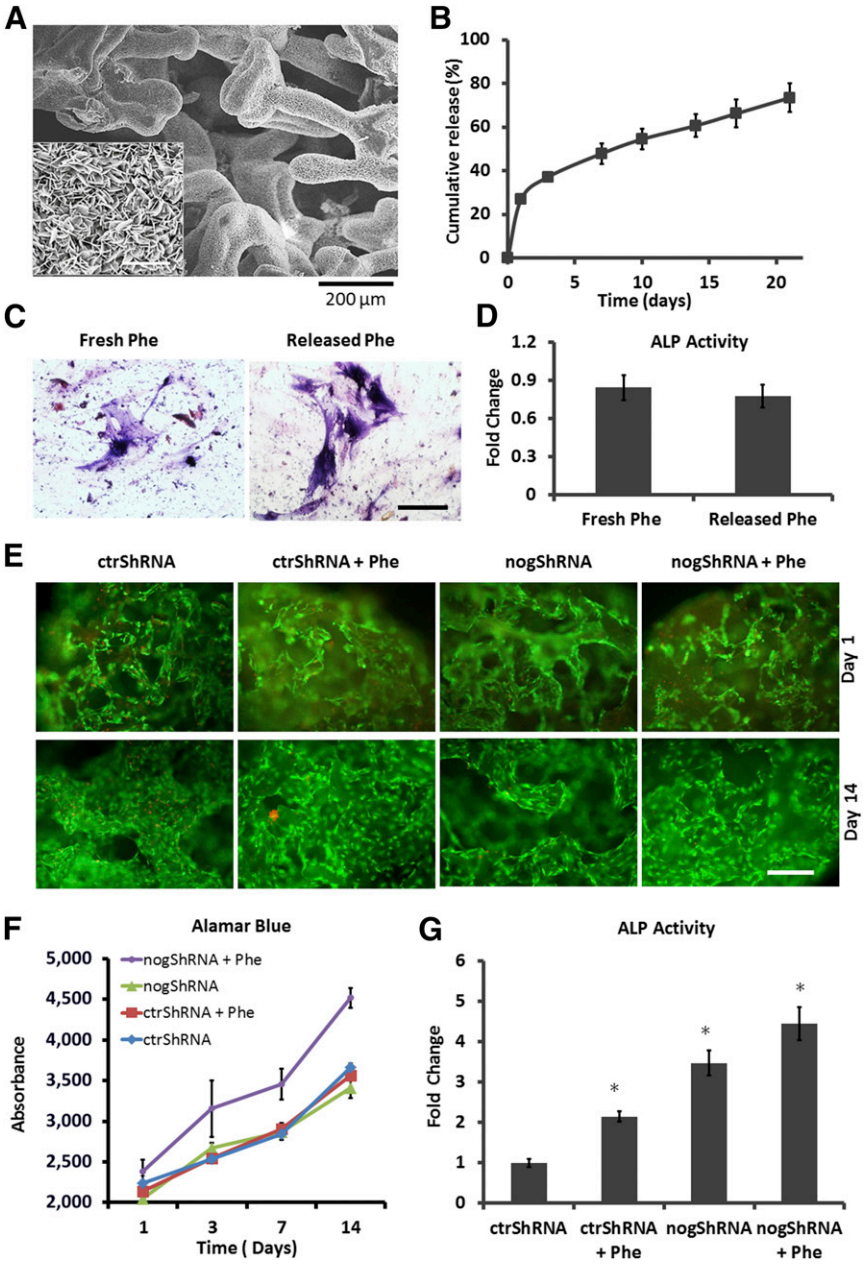

Figure 3. ASCs cultured on the Ap-PLGA scaffolds. **(A):** Scanning electron microscopic images of Ap-PLGA scaffolds. Inset shows high magnification of apatite coating. **(B):** In vitro release profile of phenamil from Ap-PLGA scaffolds. **(C, D):** Bioactivity of phenamil released from Ap-PLGA scaffolds. Scale bar = 200 μm. **(E):** Proliferation of ASCs in the Ap-PLGA scaffolds loaded with phenamil as assessed by Live-Dead fluorescent staining at days 1 and 14. Scale bar = 500 μm. **(F):** Quantification of the ASC proliferation with AlamarBlue Assay at days 1, 3, 7, and 14. **(G):** ALP activity of ASCs in Ap-PLGA scaffolds increased with noggin suppression and phenamil. Data presented as means $\pm$ SD ($n = 3$ per group). $*$, $p < .05$ versus control shRNA. Abbreviations: ALP, alkaline phosphatase; Ap-PLGA, apatite-coated poly(lactic-coglycolic acid); ASCs, adipose-derived stem cells; ALP, alkaline phosphatase; ctrShRNA, control shRNA; nogShRNA, Noggin shRNA; Phe, phenamil; shRNA, short hairpin RNA.

to BMP-responsive elements in the Id1 promoter [33, 34]. Phenamil treatment increased the Id1 luciferase activity by 1.7-fold in ASCs, which was further increased by 5.1-fold with noggin suppression compared with the control shRNA group (Fig. 2E), indicating the enhanced BMP–Smad pathway in ASCs.

ASCs Cultured on Apatite-Coated PLGA Scaffolds Releasing Phenamil

To evaluate the ability of Ap-PLGA scaffolds to support growth of noggin knockdown ASCs and deliver phenamil, three-dimensional (3D) porous PLGA scaffolds were fabricated and coated with apatite as described in our previous studies [31, 32]. A uniform layer of apatite coating with plate-like morphology was observed on the surface (Fig. 3A). The created Ap-PLGA scaffolds were loaded with phenamil (300 μM), and the release kinetic was measured by incubating the scaffolds in a PBS solution supplemented with 10% FBS. The Ap-PLGA scaffolds released phenamil in a sustained manner up to day 21, with approximately 27% of initial burst release (Fig. 3B).

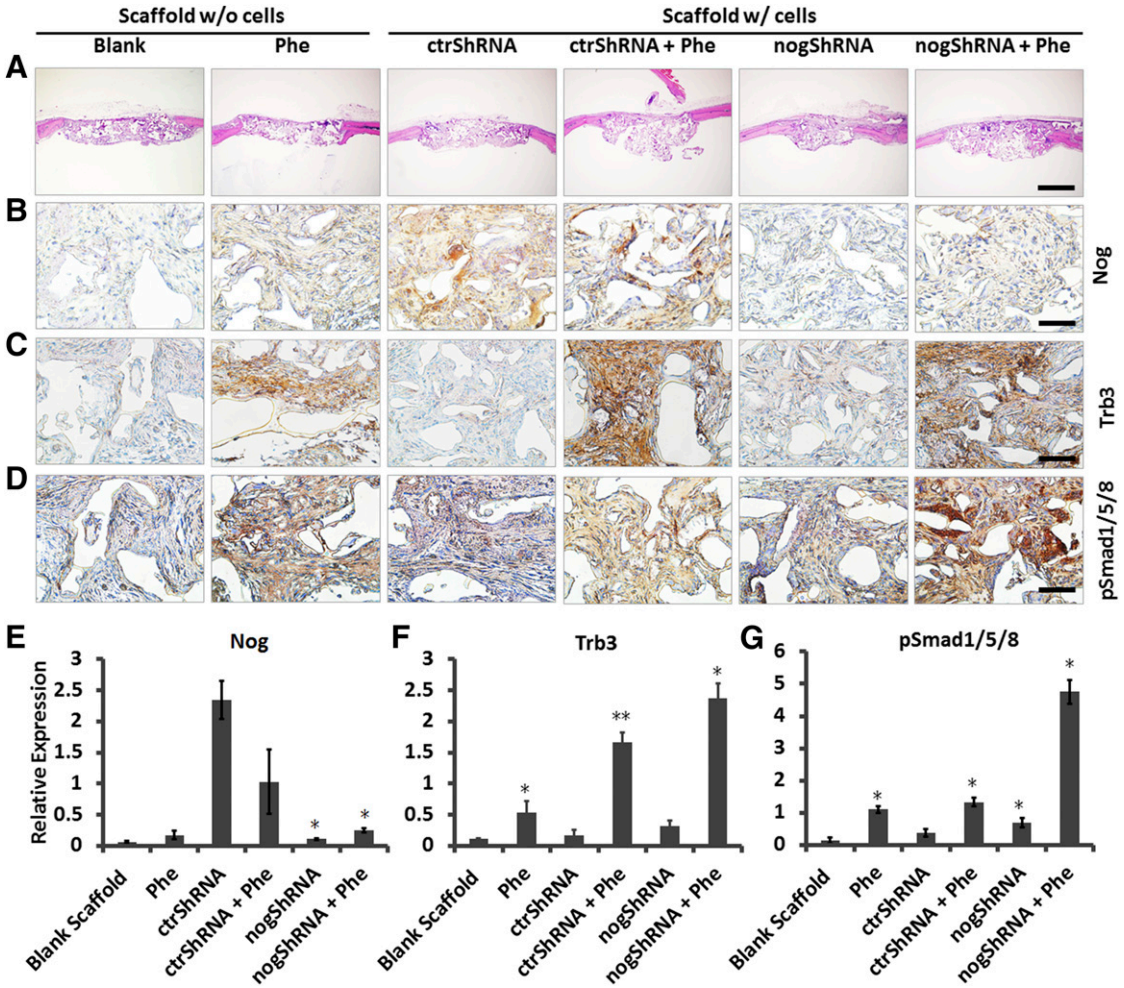

Figure 4. Noggin suppression and Phenamil accelerated BMP–Smad signaling pathway in vivo. **(A):** Histological staining of calvarial defects treated with phenamil-loaded Ap-PLGA scaffolds seeded with Noggin shRNA-transduced ASCs at 14 days postoperatively. Images were taken at ×4 magnification. Scale bar = 500 μm. **(B–D):** Immunohistochemistry staining for Noggin, Trb3, and pSmad 1/5/8 expression. Images were taken at ×40 magnification. Scale bar = 50 μm. **(E–G):** Semiquantification of immunohistochemical staining for Noggin, Trb3, and pSmad 1/5/8. Data are presented as means ± SD (n = 9 per group). *, $p < .05$, **, $p < .01$ versus blank scaffold. Abbreviations: Ap-PLGA, apatite-coated poly (lactic-coglycolic acid); ASCs, adipose-derived stem cells; BMP, bone morphogenetic protein; ctrShRNA, control shRNA; nogShRNA, Noggin shRNA; *Nog*, *Noggin*; OCN, osteocalcin; Phe, phenamil; shRNA, shRNA, short hairpin RNA; Trb3, tribbles homolog 3.

The bioactivity of phenamil released from Ap-PLGA scaffolds was determined by examining ALP expression in ASCs. The supernatant collected from phenamil-loaded scaffolds increased the ALP stain and activity of ASCs to a similar extent to that of freshly reconstituted phenamil (Fig. 3C, 3D).

To measure cell proliferation in 3D scaffold, ASCs treated with control shRNA and noggin shRNA were seeded on the scaffolds with or without phenamil and observed with Live/Dead staining (Fig. 3E). All experimental groups showed a high level of cell viability (> 95%) over the 14-day culture period. Significantly higher cell proliferation was observed in the ASCs treated with both noggin shRNA and phenamil than other groups, as indicated by AlamarBlue assay (Fig. 3F). The feasibility of Ap-PLGA scaffolds to support osteogenic differentiation was further assessed by monitoring ALP activity of ASCs seeded on the scaffolds at day 3. Noggin knockdown ASCs increased the ALP activity by 3.5-fold on the scaffolds without phenamil compared with that detected in control ASCs, which was further increased by 4.5-fold when cultured on the scaffolds loaded with phenamil (Fig. 3G).

BMP Signaling and Osteogenesis Enhanced by Noggin Suppression and Phenamil In Vivo

To examine the combined effect of the noggin suppression and phenamil on BMP signaling and subsequent osteogenesis in vivo, ASCs treated with noggin shRNA were seeded on phenamil-loaded scaffolds and implanted into critical-sized calvarial defects. There was no significant difference in bone healing among the experimental groups at 2 weeks postoperatively, although little healing was observed at the edge of the defects treated with noggin-suppressed ASCs as demonstrated by H&E and Masson's Trichrome staining (Fig. 4A; supplemental online Fig. 1).

Noggin shRNA transduction led to significant reduction in the expression level of noggin within the defects compared with the defects treated with control shRNA in the presence and absence of phenamil, as demonstrated by immunohistochemical staining for noggin (Fig. 4B, 4E). Furthermore, defects treated with phenamil significantly increased the expression of Trb3 compared with defects implanted with phenamil-free scaffolds (Fig. 4C, 4F). Lastly, noggin shRNA transduction or phenamil treatment increased

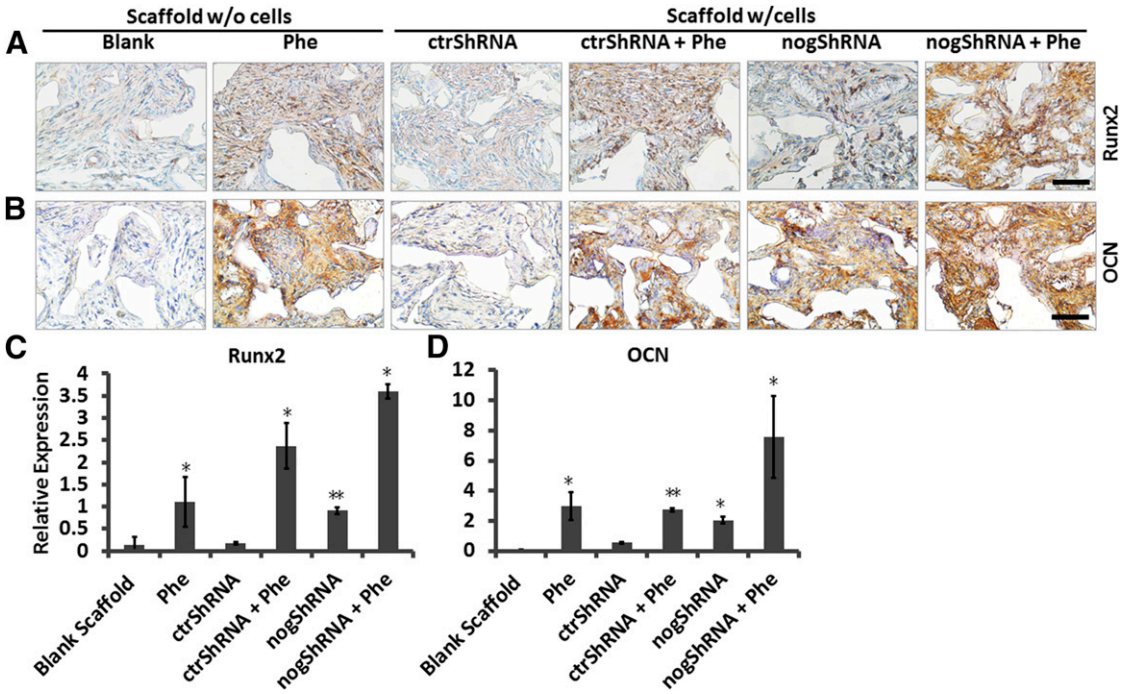

Figure 5. Noggin suppression and phenamil increased expression of osteogenic markers within calvarial defects. **(A, B):** Immunohistochemical staining for Runx2 and OCN expression in calvarial defects treated with phenamil-loaded Ap-PLGA scaffolds seeded with noggin shRNA-transduced ASCs at 14 days postoperatively. Scale bar = 50 μm. **(C, D):** Semiquantification of immunohistochemical staining for Runx2 and OCN. Data are presented as means $\pm$ SD ($n = 9$ per group). *, $p < .05$, **, $p < .01$ versus blank scaffold. Abbreviations: Ap-PLGA, apatite-coated poly(lactic-coglycolic acid); ASCs, adipose-derived stem cells; ctrShRNA, control shRNA; nogShRNA, Noggin shRNA; OCN, osteocalcin; phe, phenamil; shRNA, short hairpin RNA; w/, with; w/o, without.

BMP signaling activity as indicated by increased pSmad1/5/8 in the defects (Fig. 4D, 4G). The expression of pSmad1/5/8 was significantly higher in defects treated with both noggin shRNA transduction and phenamil compared with groups implanted with noggin knockdown ASCs or phenamil alone (Fig. 4D, 4G). In addition, the enhanced BMP activity led to increased osteogenic differentiation in defects, as demonstrated by immunohistochemical staining for osteogenic markers including Runx2 and OCN (Fig. 5A, 5B). Semiquantification of the immunohistochemical staining revealed that phenamil-releasing scaffolds seeded with noggin shRNA-transduced ASCs displayed the most intense Runx2 and OCN staining than other groups (Fig. 5C, 5D).

ASCs Enhanced Calvarial Bone Formation by Noggin Suppression and Phenamil

Lastly, we evaluated the combined effect of noggin suppression and phenamil on ASCs for bone repair in a calvarial defect model. At 6 weeks after operation, microCT images demonstrated that scaffolds seeded with noggin shRNA-transduced ASCs significantly increased calvarial healing compared with control shRNA groups (Fig. 6A). Minimal bone healing was observed in calvarial defects treated with blank scaffolds. In contrast, calvarial defects treated with phenamil-releasing scaffolds displayed enhanced bone regeneration in the presence and absence of ASCs, and almost complete bone healing was obtained after 6 weeks through combination treatment of noggin knockdown and phenamil stimulations. Moreover, only the defects in the combinatorial treatment developed a complete bone bridge crossing the defect area (Fig. 6B).

Quantification of microCT images evaluated new bone area, bone volume fraction, and trabecular number within the defects (Fig. 6C–6E). Results showed that defects treated with noggin shRNA-transduced ASCs and phenamil increased the bone healing extent to 97.5% and 65% in bone area and BV/TV after 6 weeks, whereas the calvarial defects treated with blank scaffolds showed bone healing less than 3% (Fig. 6C, 6D). Likewise, there was a significant increase in the trabecular number within the defects treated with both noggin shRNA-transduced ASCs and phenamil compared with that detected in the other experimental groups (Fig. 6E).

MicroCT findings were further confirmed by histological analysis with H&E staining (Fig. 7A) and Masson's trichrome staining (Fig. 7B). Results showed that noggin suppression + phenamil groups resulted in mature bone and thick osteoid matrix formation completely bridging and spanning the defect area after 6 weeks. Complete ossification was not apparent in defects treated with noggin shRNA-transduced ASCs or phenamil alone. In contrast to the other groups, a large amount of trabecular bone formation was observed throughout the defects treated with both noggin suppression and phenamil, as detected by Masson's trichrome staining (Fig. 7B). Collagen organization in the defect area was evaluated by PicroSirius red staining with polarized microscopy (Fig. 7C). Higher collagen deposition was observed in defects treated with noggin suppression and phenamil compared with the other groups. Birefringence of these collagen fibers resembled that of collagen fibers that are found in native calvarial bones (Fig. 7C). In addition, immunohistochemical staining for OCN, a protein associated with bone matrix mineralization, revealed that the production of OCN was increased in defects treated with noggin suppression and phenamil (Fig. 7D). In particular, the defects treated with phenamil in presence or absence

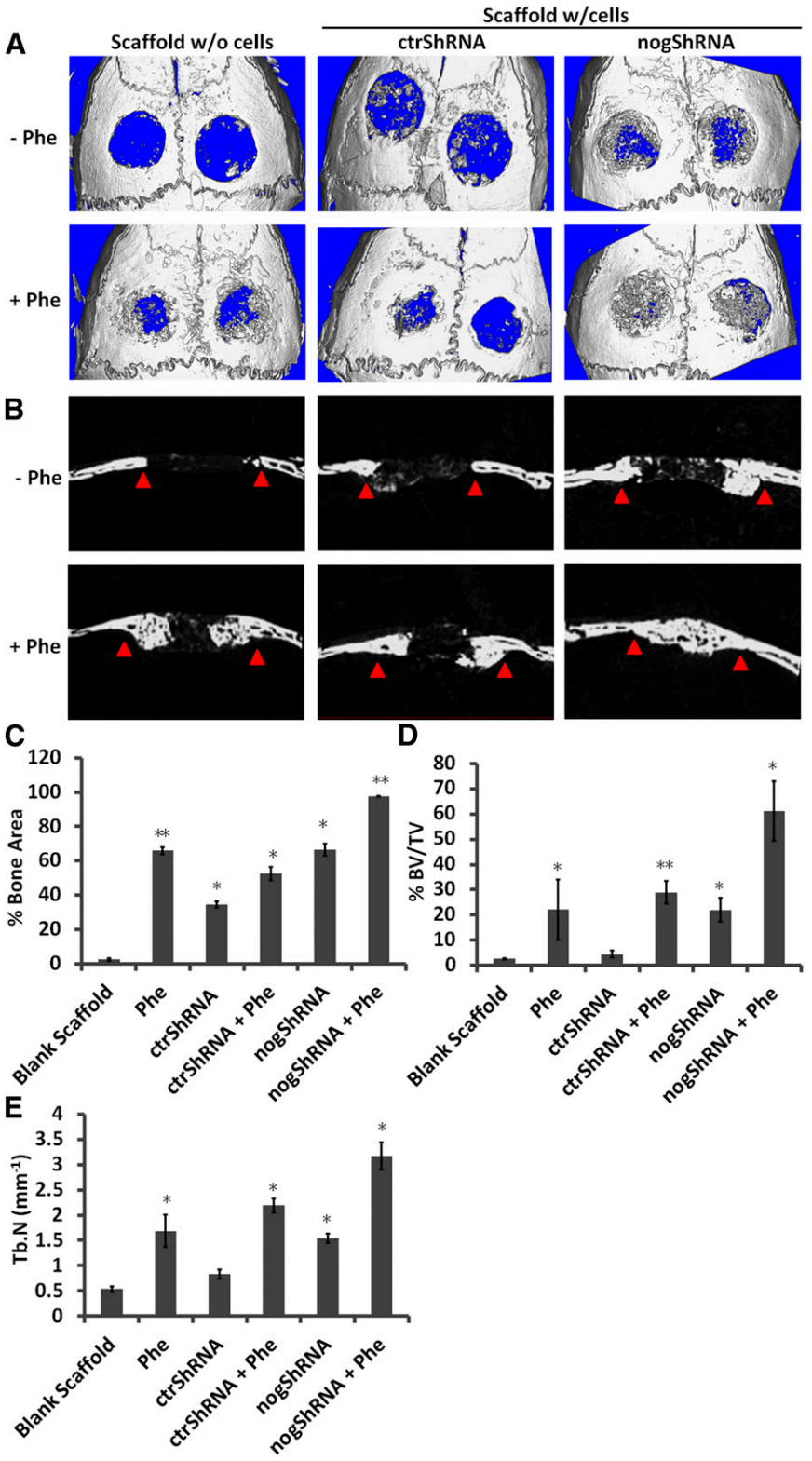

Figure 6. Noggin suppression and phenamil enhanced calvarial bone repair. **(A):** microCT images of calvarial defects treated with phenamil-loaded Ap-PLGA scaffolds seeded with noggin shRNA-transduced ASCs at 6 weeks postoperatively. **(B):** Sagittal microCT images. Arrowhead indicates approximate margins of bone defects. **(C):** Quantification of percent bone area. **(D):** Quantification of percent BV/TV. **(E):** Quantification of Tb.N (mm^{-1}). Data are presented as means ± SD ($n = 10$ per group). ∗, $p < .05$, ∗∗, $p < .01$ versus blank scaffold. Abbreviations: Ap-PLGA, apatite-coated poly(lactic-coglycolic acid); ASCs, adipose-derived stem cells; BV/TV, bone volume/tissue volume; microCT, microcomputed tomography; ctrShRNA, control shRNA; nogShRNA, Noggin shRNA; Phe, phenamil; shRNA, short hairpin RNA; Tb.N, trabecular number; w/, with; w/o, without.

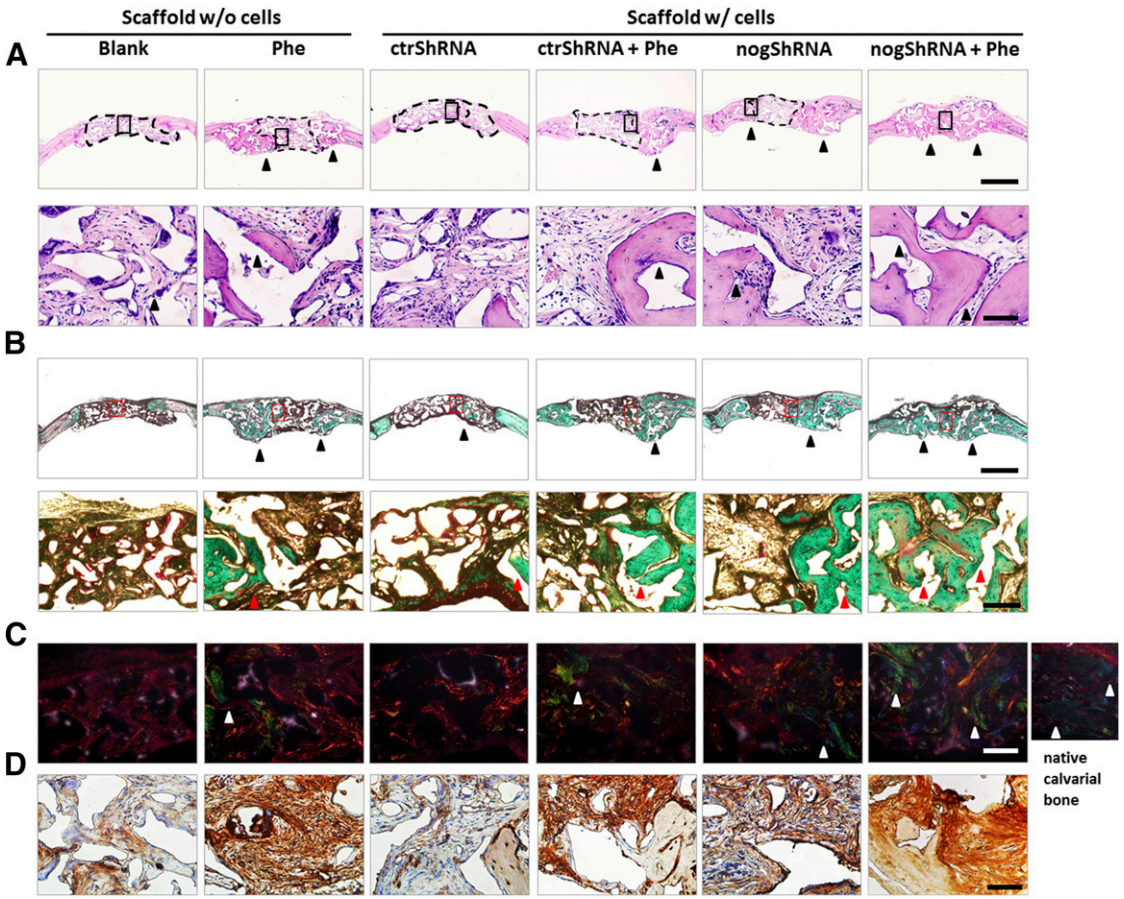

Figure 7. Histological and immunohistochemical analysis of bone regeneration in calvarial defects treated with noggin suppression and phenamil. **(A):** Histological staining of calvarial defects treated with phenamil-loaded Ap-PLGA scaffolds seeded with noggin shRNA-transduced ASCs at 6 weeks postoperatively. Dashed lines indicate relative nonhealing area. Arrowhead indicates new bone tissues. Area within the black box indicates the high magnification of image below. Images were taken at ×4 (top image) and ×40 (bottom image) magnification. Scale bars = 500 μm (top) and 50 μm (bottom). **(B):** Masson's trichrome staining. Area within the red box indicates the high magnification of the image below. Images were taken at ×4 magnification for top image and ×20 magnification for bottom image. Scale bars = 500 μm (top) and 100 μm (bottom). **(C):** Sirius red staining at polarized light. Arrowhead indicates the expression of collagen that normally exists in native calvarial bone. Images were taken at ×40 magnification. Scale bar = 50 μm. **(D):** Immunohistochemical staining for OCN. Images were taken at ×40 magnification. Scale bar = 50 μm. Abbreviations: Ap-PLGA, apatite-coated poly(lactic-coglycolic acid); ASCs, adipose-derived stem cells; ctrShRNA, control shRNA; nogShRNA, Noggin shRNA; OCN, osteocalcin; Phe, phenamil; shRNA, short hairpin RNA; w/, with; w/o, without.

of ASCs showed strong OCN production in nonbone healing area compared with blank scaffold controls (Fig. 7D).

Discussion

Current studies postulate that manipulating levels of BMP-signaling antagonists and agonists is critical to osteogenesis of ASCs. BMPs bind to and activate the receptors to phosphorylate SMAD1/5/8, which in turn are translocated into the nucleus in complex with SMAD4, ultimately regulating the transcription of the BMP target genes [6, 35]. The BMP–Smad signaling regulates stem cell self-renewal and differentiation, embryonic development, and postnatal tissue homeostasis, including bone homeostasis [6, 35]. From genetic studies in vitro and in vivo, the disruption of BMP–Smad signaling is associated with various bone-related diseases, such as osteoporosis, heterotopic ossification, and bone fracture mass [36, 37]. Thus, the BMP–Smad signaling pathway is an effective therapeutic target in the treatment of bone disorders. Our approach here is to enhance endogenous BMP–Smad activities by knocking down noggin expression in ASCs while simultaneously delivering phenamil to maximize osteoinduction and minimize potential adverse effects of current BMP-based therapeutics. Endogenous BMPs are likely to exist as heterodimeric molecules that are reported to be more potent in inducing bone formation compared with their respective homodimeric molecules [35, 36]. Given the relatively low bioactivity of recombinant BMPs and their high dose requirement in clinical applications, enhancing endogenous BMP activity through the suppression of noggin will lead to much safer and more efficient bone regeneration and is distinctly advantageous to the application of exogenous BMPs. In the present study, we demonstrated enhanced endogenous BMP signaling by downregulating noggin to promote osteogenic differentiation of ASCs and bone healing.

We further used the small molecule phenamil to complement the endogenous BMP activity mediated by noggin suppression. The small molecule phenamil was documented as a strong BMP signaling stimulator [25]. Our previous study demonstrated that phenamil additively increased osteogenic differentiation and bone repair with BMP-2 [28]. Furthermore, the

combination treatment of phenamil with BMP-2 significantly reduced the exogenous BMP-2 doses required for effective osteogenesis and bone healing. The osteogenic activity of phenamil is believed to be mediated by activation of Trb3 that stabilizes SMADs, major signal transducers for BMPs, by inhibiting the expression of BMP antagonist Smurf1 [25]. In this study, we demonstrated that the phenamil treatment can promote Trb3 expression in ASCs and calvarial defects to enhance BMP signaling and osteogenesis. The present studies also showed that phenamil treatment with noggin suppression highly enhanced BMP signaling activity in vitro and within calvarial defects compared with control shRNA or phenamil-alone groups, as demonstrated by Western blot or immunohistochemical staining for Smads. The observed bone formation was comparable to bone healing found in defects treated with BMP-2 [28], suggesting that the combined treatment of noggin suppression and phenamil may provide an efficient potential cell-based bone regeneration strategy without the need for exogenous application of supraphysiological BMP doses.

In this study, Ap-PLGA scaffolds were used to deliver noggin-suppressed ASCs and small-molecule phenamil. We have extensively studied biomimetic processing approaches to create apatite layers on the various surfaces of complex 3D scaffolds or particles including PLGA, chitosan, and tricalcium phosphate [31, 32, 38]. The apatite microenvironment created on biomaterial surfaces stimulated adipose-derived or bone marrow-derived progenitor cells to differentiate into osteoblastic cells and repaired bone defects [39, 40]. Besides promoting osteogenic activities of progenitor cells, the biomimetic apatite coating also served a favorable substrate to deliver bioactive molecules [31, 32, 38]. Our study showed that a high amount of phenamil was successfully loaded on the Ap-PLGA scaffolds, and loaded phenamil was slowly released in serum-containing medium up to 21 days. This may be because of the high surface area from the plate-like morphology of the created apatite coating, resulting in high drug retention capacity. Controlled delivery of bisphosphonate or simvastatin molecules has been reported using calcium phosphate substrates [41–43]. Furthermore, phenamil released from the Ap-PLGA scaffolds exhibited ALP activity comparable to freshly reconstituted phenamil, indicating that the bioactivity of phenamil was preserved during the loading process onto apatite layers. However, phenamil was nonspecifically adsorbed on a scaffold surface, and such physical adsorption-based delivery is often easily affected by scaffold degradation and tissue ingrowth. Given the narrow therapeutic window of phenamil, due to its hydrophobicity and dose-dependent toxicity [28], further study will be needed to better control the delivery of this molecule by developing a stand-alone nanoparticle carrier that can be integrated with the scaffolds. Moreover, the phenamil-loaded scaffold significantly enhanced proliferation and osteogenic differentiation of ASCs treated with noggin shRNA. The observed higher cell proliferation as well as osteogenic differentiation may facilitate bone healing by increasing the number of progenitor cells and the deposition of bone matrix. These results indicate that the combination treatment may be efficient for bone formation strategies in situations where maximal bone regeneration is required. However, we recognize that prolonged phenamil treatment and lack of noggin may induce undesirable tissue overgrowth or bone lesions. Additional studies on controlled delivery modalities will be needed for effective and safer deliver of phenamil and siRNA molecules.

In addition, the high BMP2 doses required for human osteogenesis are associated with life-threatening inflammatory cervical swelling and adipogenic cyst-like bone formation [44, 45]. Interestingly, Trb3 was revealed to inhibit expression of peroxisome proliferator-activated receptor γ, a master regulator of adipogenesis, and serves as a negative regulator of proinflammatory cytokines [46–48]. The additional knowledge gained from this study may suggest a new complementary osteoinductive strategy using phenamil with noggin suppression to maximize osteogenic differentiation of ASC for bone regeneration and minimize potential adverse effects of current osteoinductive therapeutics.

Conclusion

We demonstrated a strategy to enhance the BMP-signaling pathway in osteogenesis of ASCs without exogenous application of BMPs by regulating levels of antagonists and agonists to BMP signaling. The treatment of phenamil combined with the employment of noggin suppression significantly enhanced osteogenic differentiation of ASCs in vitro and calvarial bone formation in vivo through increased BMP–Smad signaling. The results indicate that the complementary approach may present novel stem cell-based therapeutic strategies in bone repair in a safe and cost-effective way.

Acknowledgments

We thank the UCLA pathology laboratory for making histological slides. This work was funded by National Institutes of Health Grants R01 AR060213 and R21 DE021819, the International Association for Dental Research, and the Academy of Osseointegration.

Author Contributions

J.F.: conception and design, collection and/or assembly of data, data analysis and interpretation, manuscript writing; C.S.I.: collection and/or assembly of data, data analysis and interpretation; M.G., Z.-K.C., A.F., S.K., N.P., and O.B.: collection and/or assembly of data; B.M.W. and C.-Y.W.: data analysis and interpretation; T.L.A.: conception and design, collection and/or assembly of data, manuscript writing; M.L.: conception and design, data analysis and interpretation, manuscript writing, final approval of manuscript.

Disclosure of Potential Conflicts of Interest

The authors indicated no potential conflicts of interest.

References

1 Burge R, Dawson-Hughes B, Solomon DH et al. Incidence and economic burden of osteoporosis-related fractures in the United States, 2005-2025. J Bone Miner Res 2007; 22:465–475.

2 Ma J, Both SK, Yang F et al. Concise review: Cell-based strategies in bone tissue engineering and regenerative medicine. Stem Cells Translational Medicine 2014;3:98–107.

3 Mizuno H, Tobita M, Uysal AC. Concise review: Adipose-derived stem cells as a novel tool for future regenerative medicine. Stem Cells 2012;30:804–810.

4 Peterson B, Zhang J, Iglesias R et al. Healing of critically sized femoral defects, using genetically modified mesenchymal stem cells from human adipose tissue. Tissue Eng 2005; 11:120–129.

5 Liao YH, Chang YH, Sung LY et al. Osteogenic differentiation of adipose-derived stem cells and calvarial defect repair using baculovirus-mediated co-expression of BMP-2 and miR-148b. Biomaterials 2014;35:4901–4910.

6 Reddi AH. Role of morphogenetic proteins in skeletal tissue engineering and

regeneration. Nat Biotechnol 1998;16: 247–252.

7 Tsuji K, Bandyopadhyay A, Harfe BD et al. BMP2 activity, although dispensable for bone formation, is required for the initiation of fracture healing. Nat Genet 2006;38:1424–1429.

8 Long F. Building strong bones: Molecular regulation of the osteoblast lineage. Nat Rev Mol Cell Biol 2012;13:27–38.

9 Kang Q, Song WX, Luo Q et al. A comprehensive analysis of the dual roles of BMPs in regulating adipogenic and osteogenic differentiation of mesenchymal progenitor cells. Stem Cells Dev 2009;18:545–558.

10 Cahill KS, Chi JH, Day A et al. Prevalence, complications, and hospital charges associated with use of bone-morphogenetic proteins in spinal fusion procedures. JAMA 2009;302:58–66.

11 Smucker JD, Rhee JM, Singh K et al. Increased swelling complications associated with off-label usage of rhBMP-2 in the anterior cervical spine. Spine 2006;31:2813–2819.

12 Lad SP, Bagley JH, Karikari IO et al. Cancer after spinal fusion: The role of bone morphogenetic protein. Neurosurgery 2013;73:440–449.

13 Brazil DP, Church RH, Surae S et al. BMP signalling: Agony and antagony in the family. Trends Cell Biol 2015;25:249–264.

14 Paine-Saunders S, Viviano BL, Economides AN et al. Heparan sulfate proteoglycans retain Noggin at the cell surface: A potential mechanism for shaping bone morphogenetic protein gradients. J Biol Chem 2002;277:2089–2096.

15 Rosen V. BMP and BMP inhibitors in bone. Ann NY Acad Sci 2006;1068:19–25.

16 Groppe J, Greenwald J, Wiater E et al. Structural basis of BMP signalling inhibition by the cystine knot protein Noggin. Nature 2002; 420:636–642.

17 Capdevila J, Johnson RL. Endogenous and ectopic expression of noggin suggests a conserved mechanism for regulation of BMP function during limb and somite patterning. Dev Biol 1998;197:205–217.

18 Gazzerro E, Gangji V, Canalis E. Bone morphogenetic proteins induce the expression of noggin, which limits their activity in cultured rat osteoblasts. J Clin Invest 1998;102:2106–2114.

19 Smith WC, Harland RM. Expression cloning of noggin, a new dorsalizing factor localized to the Spemann organizer in Xenopus embryos. Cell 1992;70:829–840.

20 Wan DC, Pomerantz JH, Brunet LJ et al. Noggin suppression enhances in vitro osteogenesis and accelerates in vivo bone formation. J Biol Chem 2007;282:26450–26459.

21 Abe E, Yamamoto M, Taguchi Y et al. Essential requirement of BMPs-2/4 for both osteoblast and osteoclast formation in murine bone marrow cultures from adult mice: Antagonism by noggin. J Bone Miner Res 2000;15:663–673.

22 Fan J, Park H, Tan S et al. Enhanced osteogenesis of adipose derived stem cells with Noggin suppression and delivery of BMP-2. PLoS One 2013;8:e72474.

23 Fan J, Park H, Lee MK et al. Adipose-derived stem cells and BMP-2 delivery in chitosan-based 3D constructs to enhance bone regeneration in a rat mandibular defect model. Tissue Eng Part A 2014;20:2169–2179.

24 Balmayor ER. Targeted delivery as key for the success of small osteoinductive molecules. Adv Drug Deliv Rev 2015;94:13–27.

25 Park KW, Waki H, Kim WK et al. The small molecule phenamil induces osteoblast differentiation and mineralization. Mol Cell Biol 2009; 29:3905–3914.

26 Kim JG, Son KM, Park HC et al. Stimulating effects of quercetin and phenamil on differentiation of human dental pulp cells. Eur J Oral Sci 2013;121:559–565.

27 Lo KW, Kan HM, Laurencin CT. Short-term administration of small molecule phenamil induced a protracted osteogenic effect on osteoblast-like MC3T3-E1 cells. J Tissue Eng Regen Med 2013.

28 Fan J, Im CS, Cui ZK et al. Delivery of phenamil enhances BMP-2-induced osteogenic differentiation of adipose-derived stem cells and bone formation in Calvarial Defects. Tissue Eng Part A 2015;21:2053–2065.

29 Chan MC, Nguyen PH, Davis BN et al. A novel regulatory mechanism of the bone morphogenetic protein (BMP) signaling pathway involving the carboxyl-terminal tail domain of BMP type II receptor. Mol Cell Biol 2007;27: 5776–5789.

30 Khattab HM, Ono M, Sonoyama W et al. The BMP2 antagonist inhibitor L51P enhances the osteogenic potential of BMP2 by simultaneous and delayed synergism. Bone 2014;69:165–173.

31 Chou YF, Dunn JC, Wu BM. In vitro response of MC3T3-E1 pre-osteoblasts within three-dimensional apatite-coated PLGA scaffolds. J Biomed Mater Res B Appl Biomater 2005;75:81–90.

32 Park H, Choi B, Nguyen J et al. Anionic carbohydrate-containing chitosan scaffolds for bone regeneration. Carbohydr Polym 2013;97: 587–596.

33 Hayashi M, Nimura K, Kashiwagi K et al. Comparative roles of Twist-1 and Id1 in transcriptional regulation by BMP signaling. J Cell Sci 2007;120:1350–1357.

34 Valdimarsdottir G, Goumans MJ, Rosendahl A et al. Stimulation of Id1 expression by bone morphogenetic protein is sufficient and necessary for bone morphogenetic protein-induced activation of endothelial cells. Circulation 2002; 106:2263–2270.

35 Wagner DO, Sieber C, Bhushan R et al. BMPs: From bone to body morphogenetic proteins. Sci Signal 2010;3:mr1.

36 Urist MR. Bone: Formation by autoinduction. Science 1965;150:893–899.

37 Kaplan FS, Xu M, Seemann P et al. Classic and atypical fibrodysplasia ossificans progressiva (FOP) phenotypes are caused by mutations in the bone morphogenetic protein (BMP) type I receptor ACVR1. Hum Mutat 2009;30:379–390.

38 Hu J, Hou Y, Park H et al. Beta-tricalcium phosphate particles as a controlled release carrier of osteogenic proteins for bone tissue engineering. J Biomed Mater Res A 2012;100: 1680–1686.

39 Cowan CM, Shi YY, Aalami OO et al. Adipose-derived adult stromal cells heal critical-size mouse calvarial defects. Nat Biotechnol 2004;22:560–567.

40 Chou YF, Huang W, Dunn JC et al. The effect of biomimetic apatite structure on osteoblast viability, proliferation, and gene expression. Biomaterials 2005;26:285–295.

41 Chou J, Ito T, Bishop D et al. Controlled release of simvastatin from biomimetic β-TCP drug delivery system. PLoS One 2013;8:e54676.

42 Pascaud P, Errassifi F, Brouillet F et al. Adsorption on apatitic calcium phosphates for drug delivery: Interaction with bisphosphonate molecules. J Mater Sci Mater Med 2014;25: 2373–2381.

43 Josse S, Faucheux C, Soueidan A et al. Novel biomaterials for bisphosphonate delivery. Biomaterials 2005;26:2073–2080.

44 Perri B, Cooper M, Lauryssen C et al. Adverse swelling associated with use of rh-BMP-2 in anterior cervical discectomy and fusion: A case study. Spine J 2007;7:235–239.

45 Vaidya R, Carp J, Sethi A et al. Complications of anterior cervical discectomy and fusion using recombinant human bone morphogenetic protein-2. Eur Spine J 2007;16: 1257–1265.

46 Takahashi Y, Ohoka N, Hayashi H et al. TRB3 suppresses adipocyte differentiation by negatively regulating PPARgamma transcriptional activity. J Lipid Res 2008;49:880–892.

47 Bezy O, Vernochet C, Gesta S et al. TRB3 blocks adipocyte differentiation through the inhibition of C/EBPbeta transcriptional activity. Mol Cell Biol 2007;27:6818–6831.

48 Borsting E, Patel SV, Declèves AE et al. Tribbles homolog 3 attenuates mammalian target of rapamycin complex-2 signaling and inflammation in the diabetic kidney. J Am Soc Nephrol 2014;25:2067–2078.

See www.StemCellsTM.com for supporting information available online.

